Supporting information

Single stranded 1D-helical Cu coordination polymer for ultra-sensitive ammonia sensing at room temperature

Taehun Im,[ac] Juyun Lee,[abc] Sung-Chul Kim,[d] Joharimanitra Randrianandraina,[e] Joo-Won Lee,[a] Myoung Won Chung,[f] Taesung Park,[c] Kam-Hung Low,[g] Seungkyu Lee,[g] Soong Ju Oh,[c] Yun Chan Kang,[c] Seunghyun Weon,[f] Jung-Hoon Lee,[e] Seon Joon Kim,[*abh] and Sohee Jeong[*a]

[a]Materials Architecturing Research Center, Korea Institute of Science and Technology, Seoul, 02792, South Korea.

[b]Convergence Research Center for Solutions to Electromagnetic Interference in Future-mobility, Korea Institute of Science and Technology, Seoul 02792, Republic of Korea.

[c]Department of Materials Science and Engineering, Korea University, Seoul, 02841, Republic of Korea.

[d]Advanced Analysis and Data Center, Korea Institute of Science and Technology, Seoul 02792, Republic of Korea.

[e]Computational Science Research Center, Korea Institute of Science and Technology, Seoul 02792, Republic of Korea.

[f]School of Health and Environmental Science & Department of Health and Safety Convergence Science, Korea University, Seoul, 02841, Korea.

[g]Department of Chemistry, The University of Hong Kong, Pokfulam Road, Hong Kong SAR, China.

[h]Division of Nanoscience and Technology, KIST School, University of Science and Technology, Seoul 02792, Republic of Korea.

Supplementary Note 1. Materials and Methods

Materials

Copper(II) chloride ($CuCl_2$, 97%, Sigma-Aldrich), N-methylthiourea (98%, Tokyo Chemical Industry Co.), Ethyl alcohol anhydrous (99.9%, Samchun Chemicals), Silver nitrate soultion (2.5% w/v $AgNO_3$ in H_2O, Sigma-Aldrich)

Synthesis of MTCP and Ag-MTCP

In a typical experiment, 33.5 mg of *N*-Methylthiourea (33.5mg) was dissolved in 50 mL ethanol. After full dissolvation, 50 mg of $CuCl_2$ was added and left to react for 10 minutes while stirring at room temperature. Then, the solution was centrifuged at 6000 rpm for 5 minutes to collect the product. For the synthesis of Ag-MTCP, synthesized MTCP was dispersed in 50 mL ethanol and sonicated until a homogeneous dispersion was obtained. Then, 0.087 mL $AgNO_3$ was added and stirred for 2 hours. Finally, Ag-MTCP was obtained after washing the solution twice by centrifugation at 6000 rpm for 5 minutes.

Preparation of gas sensors and sensing measurements

Gas sensing electrodes were prepared by depositing Au/Ti patterns onto SiO_2/Si wafer substrates, which was cleansed by bath sonication with ethanol and IPA for 30 minutes, respectively. Then, small amounts of MTCP or Ag-MTCP dispersed in ethanol was dropped onto the gas sensing electrodes while heating the substrate at 55°C to dry the solvent. Deposited electrodes were then placed in a leak-tight homemade gas sensing chamber, and all measurements were performed at room temperature. The electrical resistance of MTCP deposited electrodes were measured and recorded in real-time using a sourcemeter (Keithley 2400) while flowing nitrogen gas mixed with target analytes through the gas sensing chamber. Target gases with various concentrations and humidity were configured by controlling the flow rates between the target analyte, dry baseline gas, and humid baseline gas using mass flow controllers. Unless mentioned otherwise, gas sensing data was obtained in a dry condition.

Crystal Structure Determination by Single-Crystal X-ray Diffraction

Crystals suitable for SCXRD experiment were mounted on a MiTeGen dual-thickness micro-mount and placed under a cold stream of nitrogen (Oxford Cryostream 800) at 173 K. Measurements were recorded on a Bruker D8 VENTURE Duo FIXED-CHI X-Ray Diffractometer using a IµS micro-focus Mo-Kα radiation ($\lambda = 0.71073$ Å) with a Quazar multilayer optics. Data collection was conducted with the APEX3 v2019.3-2click4 (Bruker Nano, 2019) program. Cell refinement and data reduction were performed with the SAINT V8.38A (Bruker AXS Inc., 2017) program. The structure was solved using XT 2014/5 in the APEX3 suite and refined with SHELXL2018/3.[1, 2] Hydrogen atoms were placed in idealized positions and were set riding on the respective parent atoms. All non-hydrogen atoms were refined with anisotropic thermal parameters. The structure was refined by weighted least squares refinement on F2 to convergence. All e.s.d.'s (except the e.s.d. in the dihedral angle between two least-square planes) are estimated using the full covariance matrix. The X-ray crystallographic data of MTCP has been deposited at the Cambridge Crystallographic Data Centre (CCDC), under the deposition number CCDC 2301059. The data can be obtained free of charge from the Cambridge Crystallographic Data Center (https://www.ccdc.cam.ac.uk/structures/).

In-situ diffuse reflectance infrared Fourier transform spectroscopy (DRIFTs)

In-situ DRIFTS was conducted using a Spectrum 3 spectrometer (PerkinElmer, Inc., Waltham, Massachusetts, USA) equipped with an in-situ diffuse-reflectance cell (DiffusIR, PIKE Technologies, Madison, Wisconsin, USA). The samples were placed in the cell and flushed with N_2 for 30 min. NH_3 (300 ppm) in N_2 (balance) was introduced into the cell at RT. DRIFTS spectra were collected after exposing the samples to the flowing stream for 1, 3, 5, 7, and 10 min.

Supplementary Note 2. Characterization

Transmission Electron Microscopy (TEM): STEM and TEM images were acquired through Talos F200X (FEI company). Scanning Electron Microscopy (SEM): SEM images were obtained using Inspect F (FEI company) and Regulus 8230 (Hitachi). Powder X-ray Diffraction Spectroscopy (PXRD): The powder X-ray diffraction patterns were obtained using D8 ADVANCE (Bruker) with a Cu-Kα radiation (λ = 1.5418 Å; 40 kV, 40 mA) in the range of 5 to 60 degree with 1 degree/min scanning speed. X-ray Photoelectron Spectroscopy (XPS): The XPS results were obtained using Nexsa (ThermoFisher Scientific) equipped with Microfocus monochromatic X-ray source (Al-K (1486.6 eV)). Fourier-transform infrared spectroscopy (FTIR): The FTIR Results were obtained using NICOLET iS10 (ThermoFisher Scientific). Atomic Force Microscopy (AFM): The AFM images were obtained using Park XE-7 (Park system). The raw AFM images were processed using XEI 4.3.0 software. Ultraviolet-visible spectroscopy (UV-Vis) transmittance and absorbance: The reflectance spectra were acquired using UV-2600(Shimadzu). Ultraviolet photoelectron spectroscopy (UPS): Work function and valence band maximum were obtained using Nexsa (ThermoFisher Scientific) equipped with source (He I (21.22eV)). Focused ion beam (FIB): Samples fabricated to measure the conductivity with the assistance of FIB were prepared by Quanta 3D FEG (FEI company). X-ray absorption spectroscopy (XAS): Cu K-edge and L-edge XAS, XANES were collected on the 1D and 10D beam line at the Pohang Accelerator Laboratory (PAL).

Supplementzry Note 3. Computational methods

To understand NH_3 adsorption mechanisms in MTCP, we performed first-principles density functional theory (DFT) calculations using-the Vienna Ab initio Simulation Package code (VASP 6.1) with the Revised Perdew-Burke-Ernzerhof (RPBE) exchange correlation functional, complemented by the Hubbard U correction (6.5 eV) for Cu 3d orbital. To accurately describe van der Waals interactions, we performed geometry optimization and energy minimization with Grimme's D3 dispersion correction. Γ-point sampling was used to sample the Brillouin zone. The plane wave cutoff energy was set at 520 eV. For static DFT calculations, force and energy convergence criteria were set to 0.01 eV/Å and 10^{-7} eV respectively. The binding energies (E_{ads}) were calculated as follow:

$$E_{ads} = E_{MTCP + NH_3} - (E_{MTCP} + E_{NH3})$$

where $E_{MTCP+NH3}$ and E_{MTCP} represent the total energies of a 1×1×2 supercell (a=b=11.2Å, c=14.35Å; α=β=γ=90°) of MTCP with and without NH_3 molecules and E_{NH3} is the total energy of a NH_3 gas molecule in a 20 Å × 20 Å × 20 Å cubic supercell.

To find additional stable adsorption sites of NH_3, we also performed ab initio Molecular Dynamics (AIMD) in the NVT ensemble over a minimum period of 10 ps at variable temperatures in range of between 300 and 500 K regulated with the Andersen thermostat. The electronic parameters used for static DFT relaxation were also set for AIMD. During static relaxation, all of the atom positions, cell shape and cell volume were allowed to vary.

Supplementary figures and tables

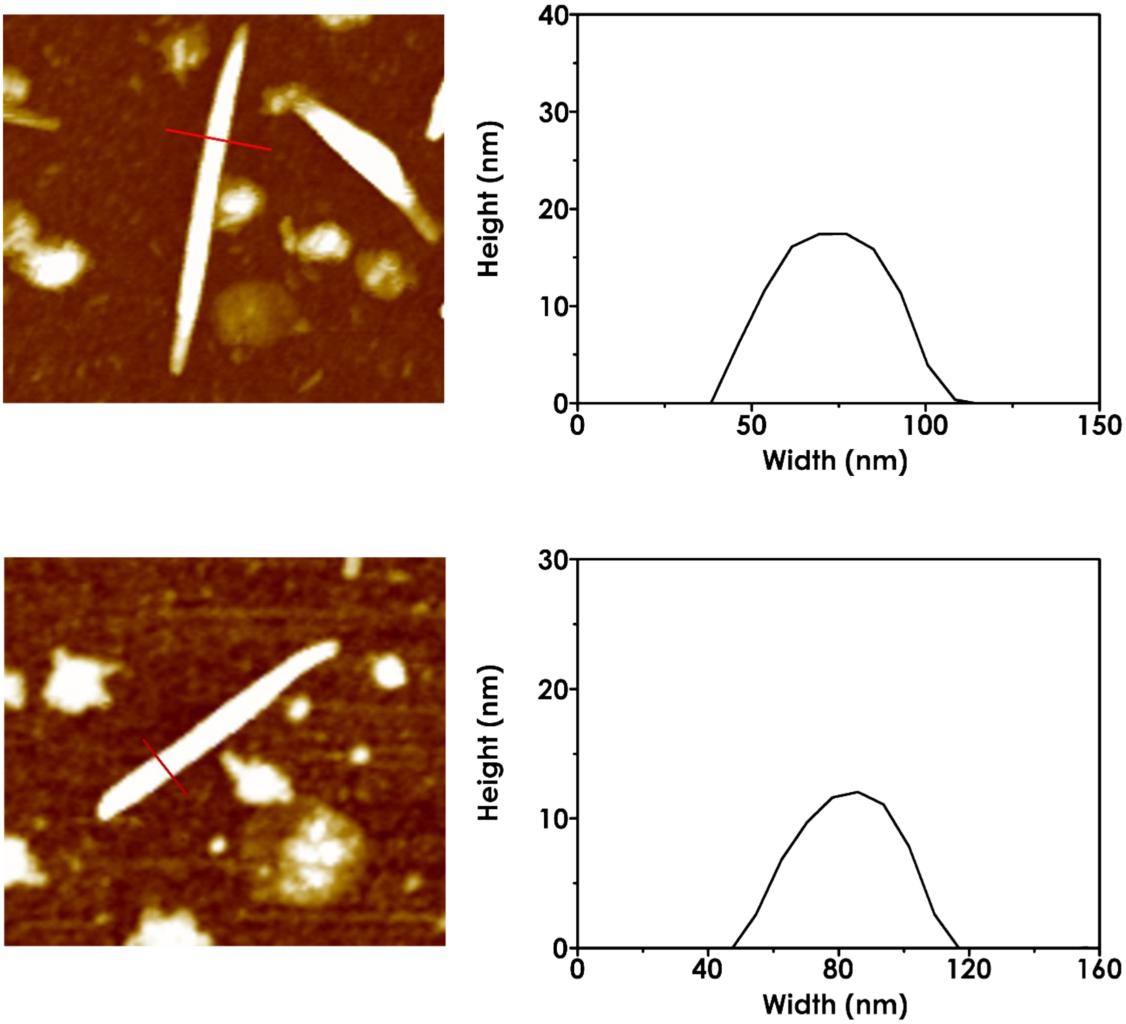

Figure S1. AFM image of MTCP. It is confirmed that the observed nanowires had a 13~17 nm thickness and had an elliptical cross-section.

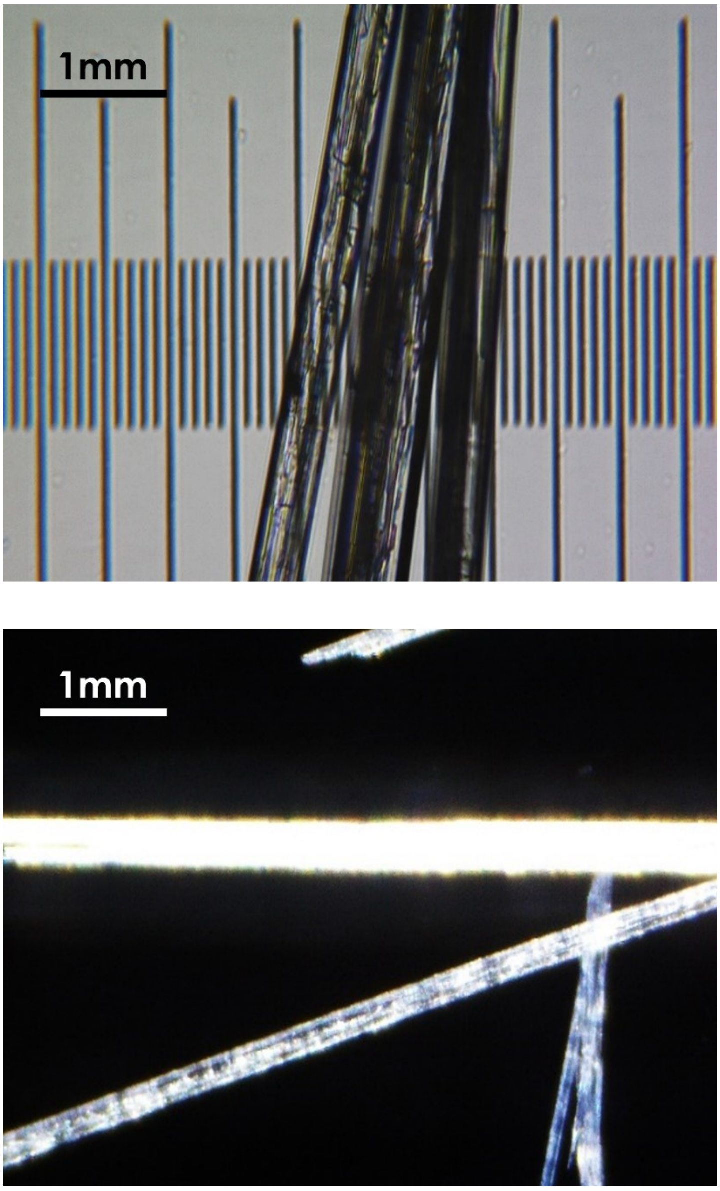

Figure S2. MTCP crystals observed under an optical microscope.

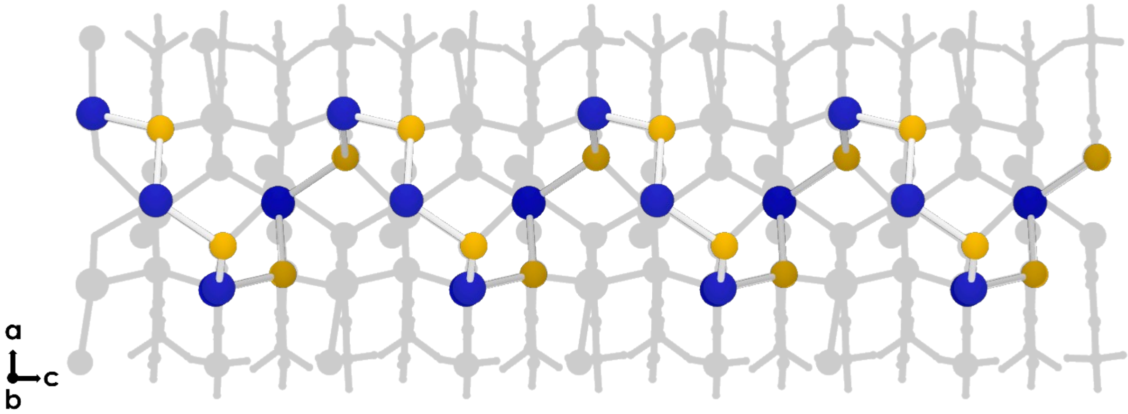

Figure S3. The 1D-helical structural model of MTCP illustrate screw symmetry. In this structure, the highlighted chain is replicated on the opposite side in a repetitive manner.

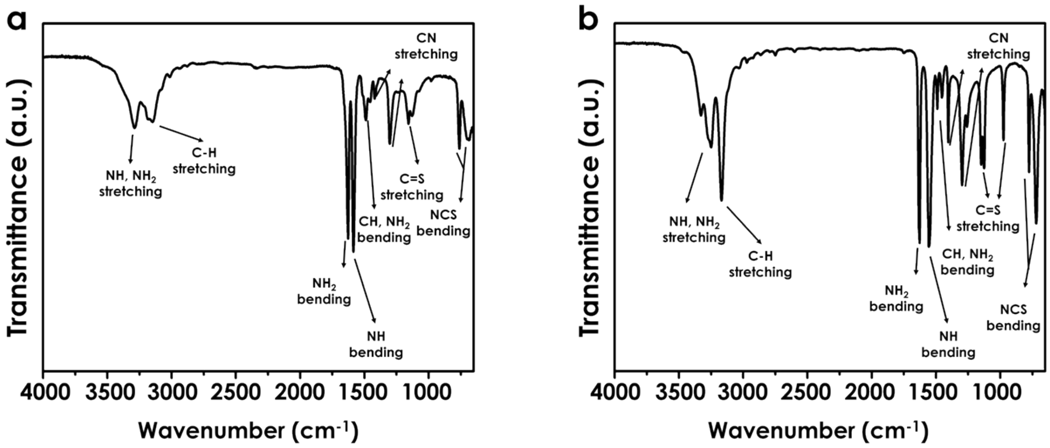

Figure S4. FTIR spectra of (a) MTCP and (b) MT precursor.

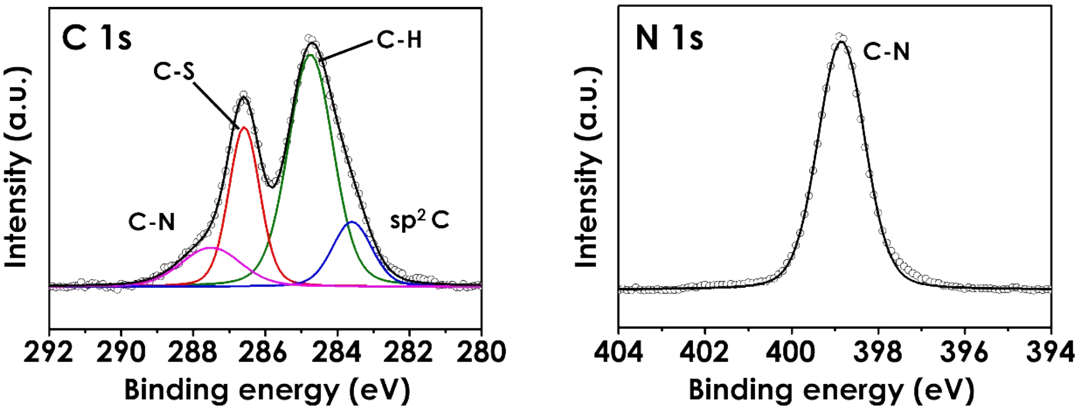

Figure S5. XPS spectra of MTCP at the C 1s and N 1s core regions. Peaks were calibrated using the C-H bonds (284.8 eV).

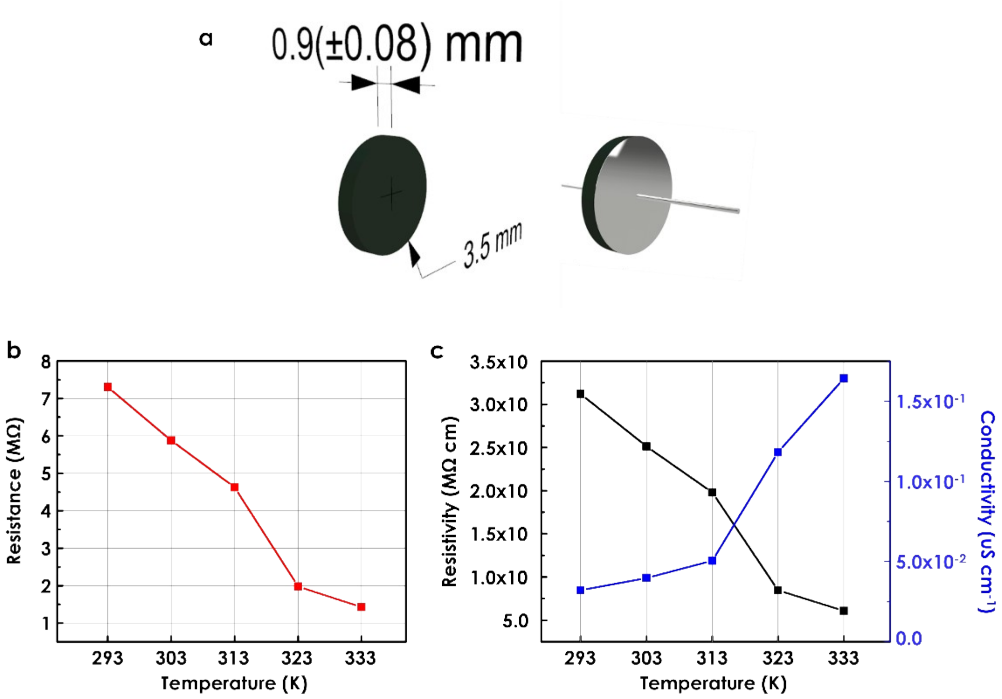

Figure S6. (a) Schematic of the 2-point probe current measurement technique. In the measurements, MTCP powder was meticulously prepared using a 7 mm pellet die, subsequently fabricated into a cylindrical pellet of dimensions 7 mm (diameter) x 0.9 mm (±0.08 mm) (height). (b) Resistance of MTCP pellet at different temperature. Temperature was manipulated in increments of 10 K step, spanning the range from 293K to 333 K. (c) Resistivity and conductivity at different temperatures calculated with resistance values.

The TCR value was calculated by the following equation.

$$TCR = \frac{\Delta\rho}{\rho_i \Delta T}$$

(ρ_i: initial resistivity, $\Delta\rho$: changes of the resistivity ΔT: changes of the temperature)

Measured resistivity of MTCP were determined as 3.12 x 10^1 MΩcm at 293 K, and 0.61 x 10^1 MΩcm at 333 K.

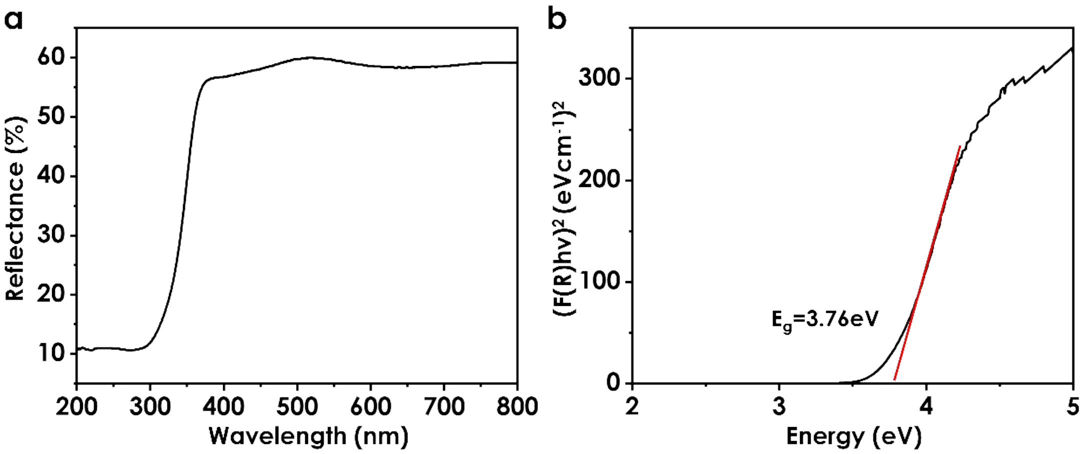

Figure S7. (a) UV-vis reflectance of MTCP powder. (b) Tauc plot and band gap of MTCP by measured using UV-vis data.

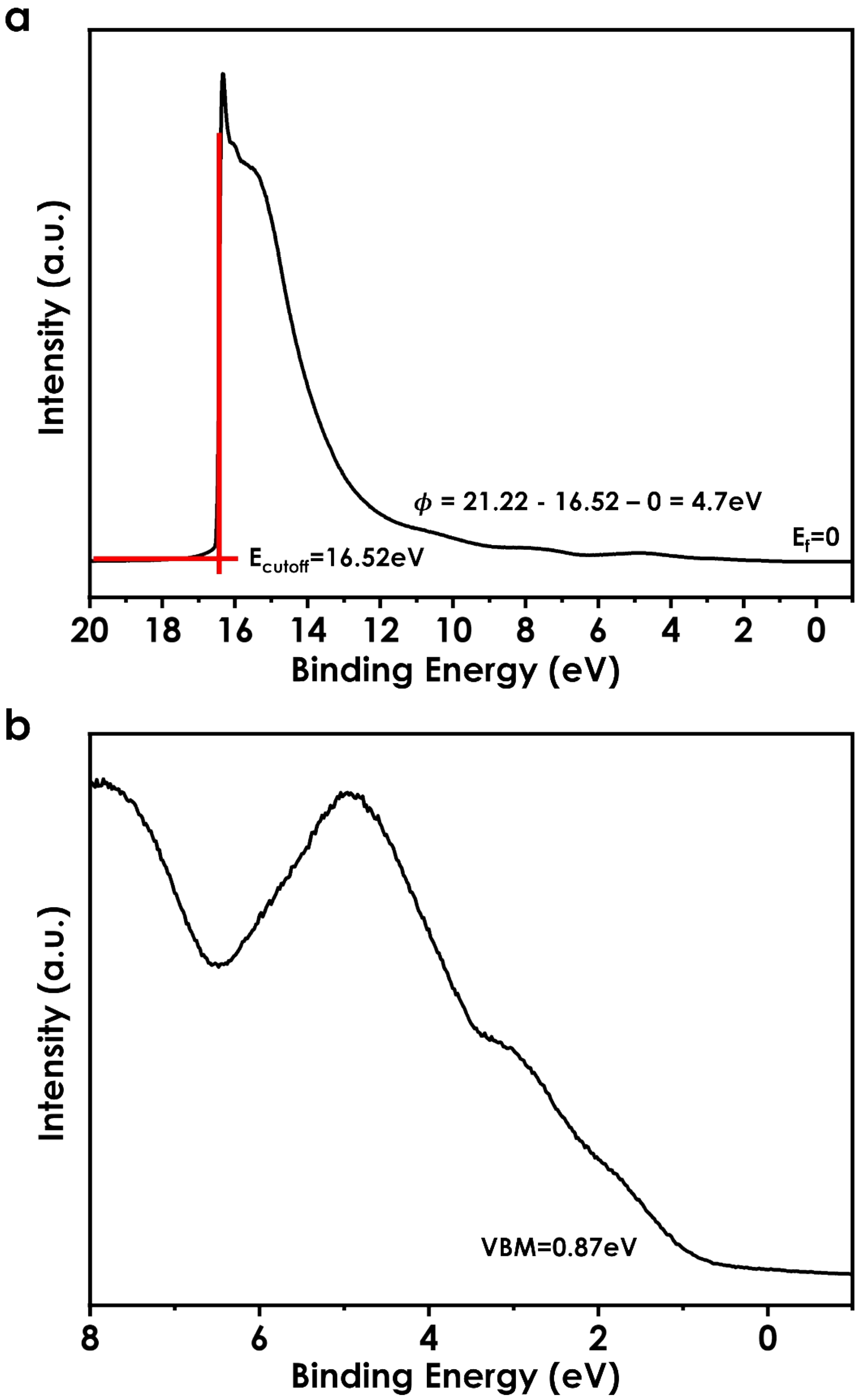

Figure S8. UPS measurements of MTCP. (a) Work function, (b) valence band maximum of MTCP.

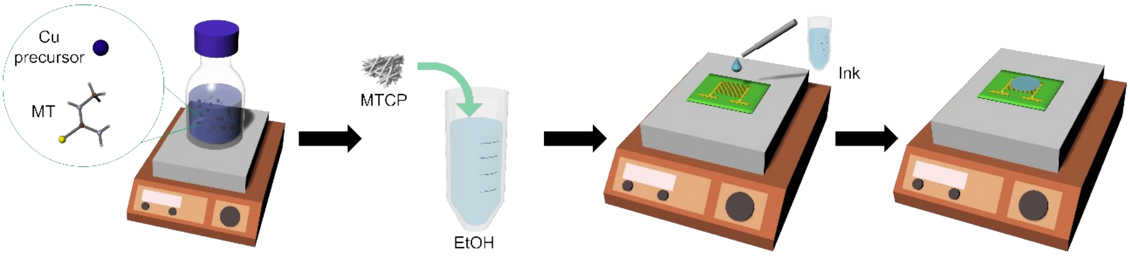

Figure S9. Schematic diagram of gas sensor manufacturing process

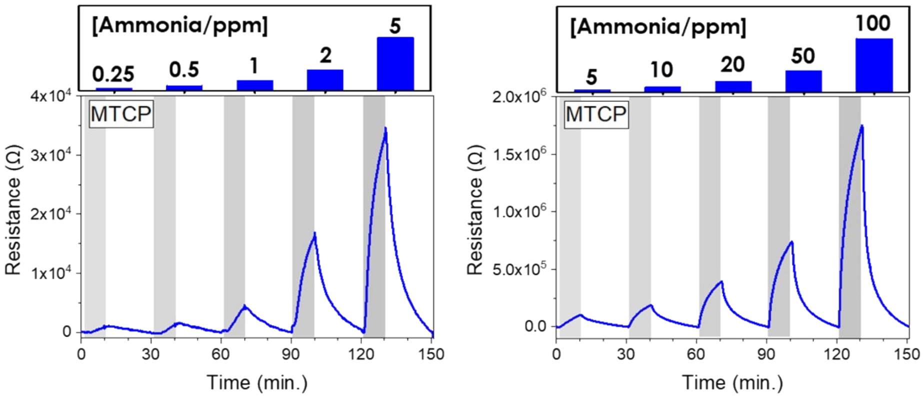

Figure S10. Electrical resistance change of MTCP towards 0.25-5 ppm NH_3 and 5-100 ppm NH_3.

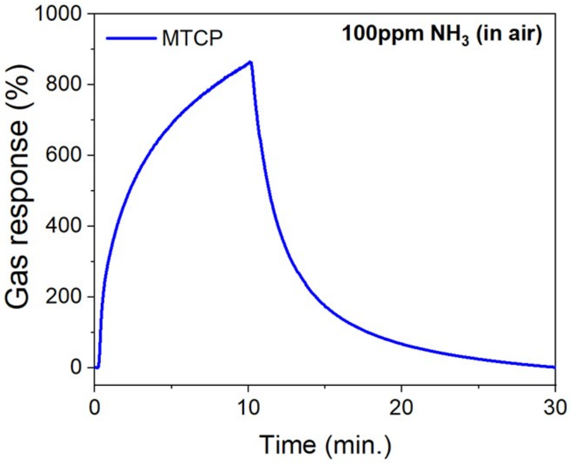

Figure S11. Dynamic gas response of MTCP toward 100 ppm NH_3 in a dry air environment.

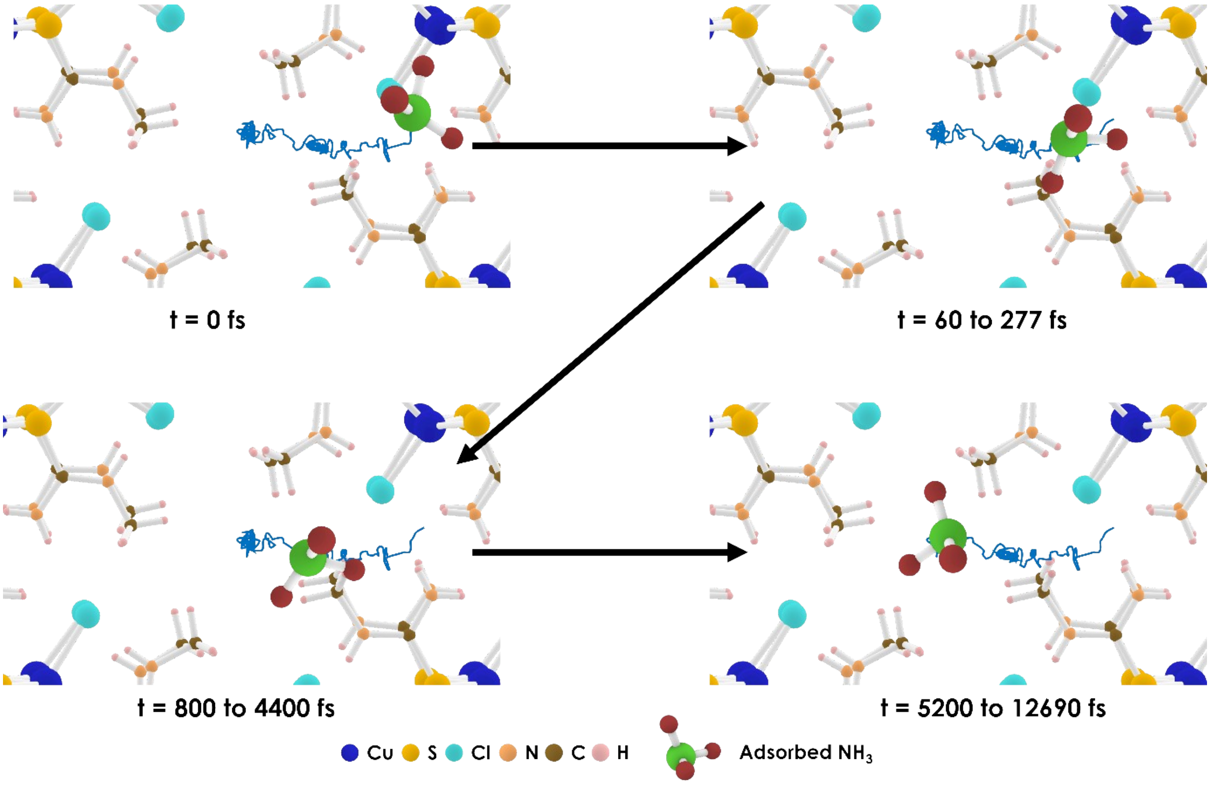

Figure S12. The AIMD-trajectory of NH_3 toward finding the most stable adsorption site.

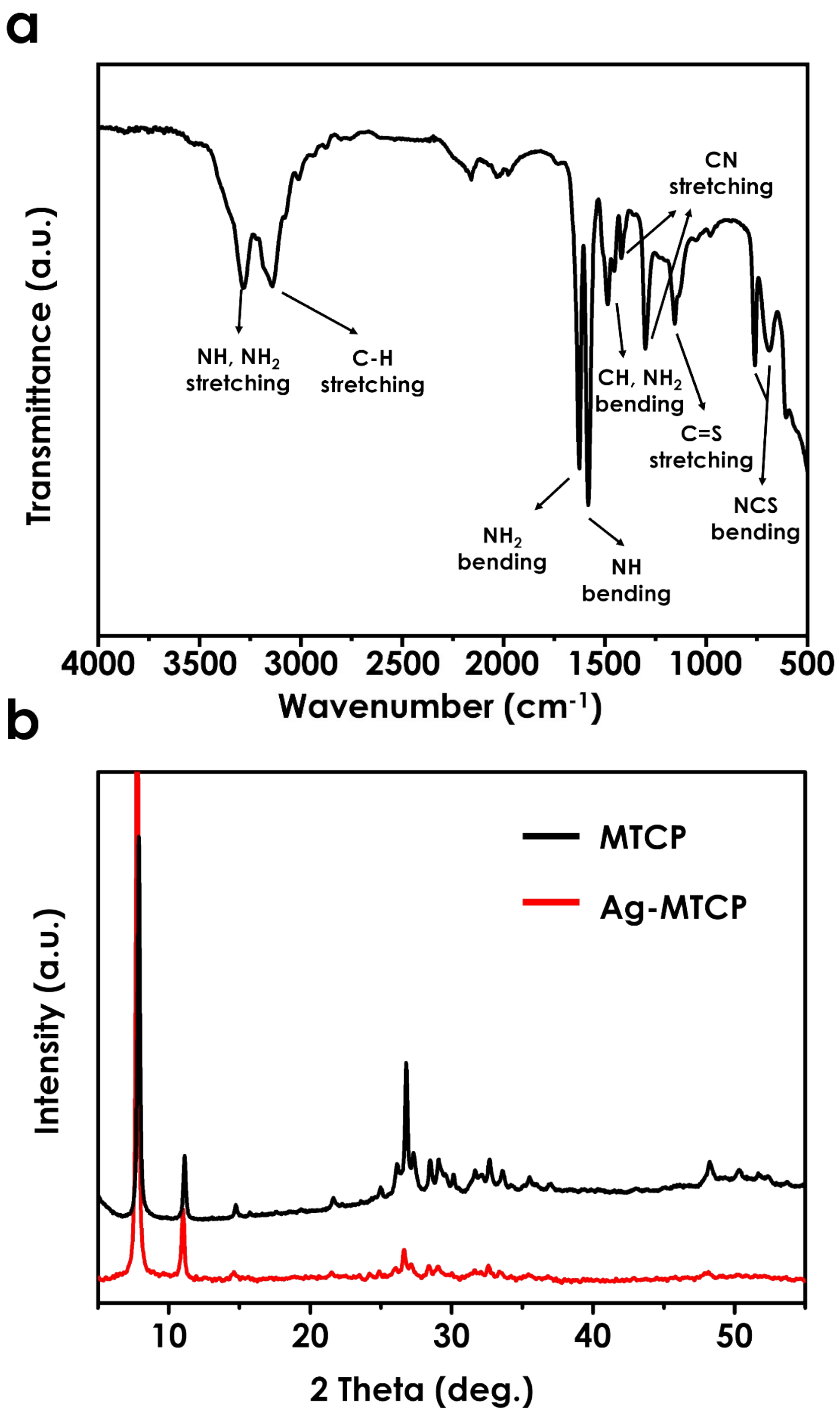

Figure S13. (a) FTIR spectrum of Ag-MTCP and (b) XRD comparison between MTCP and Ag-MTCP.

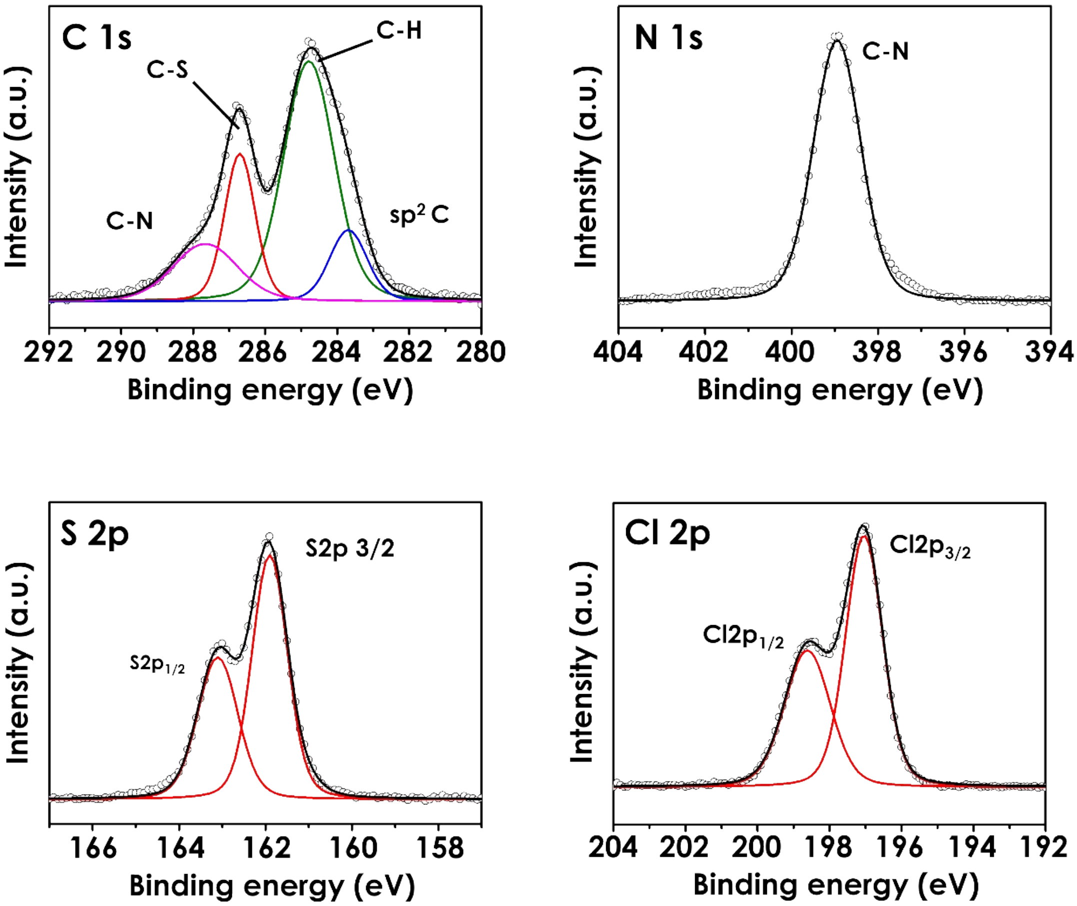

Figure S14. XPS spectra of synthesized Ag-MTCP.

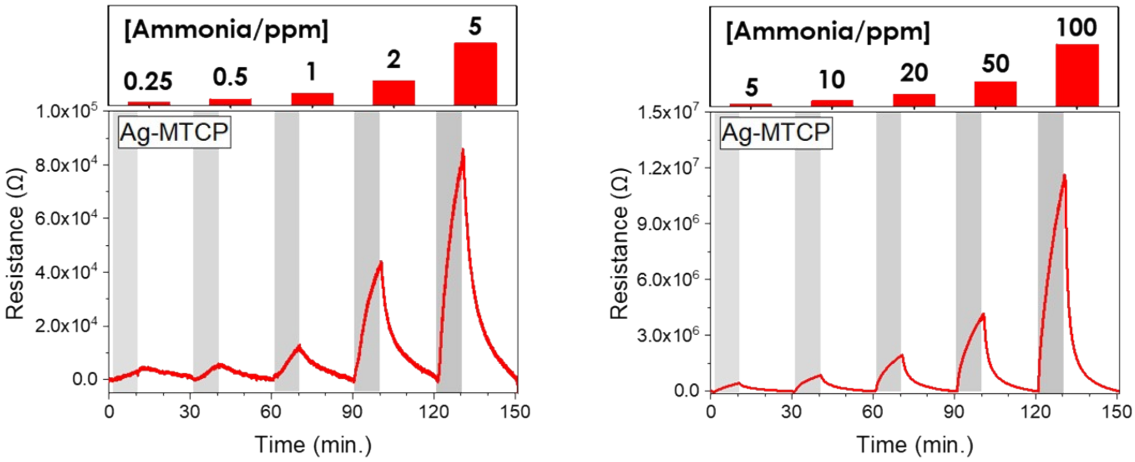

Figure S15. Electrical resistance change of Ag-MTCP towards 0.25-5 ppm NH_3 and 5-100 ppm NH_3.

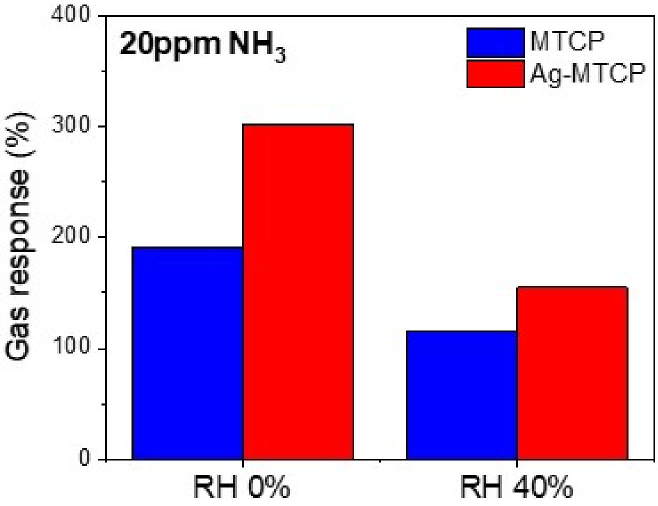

Figure S16. Gas response of MTCP and Ag-MTCP sensor toward 20 ppm NH_3 under dry and 40% RH environment.

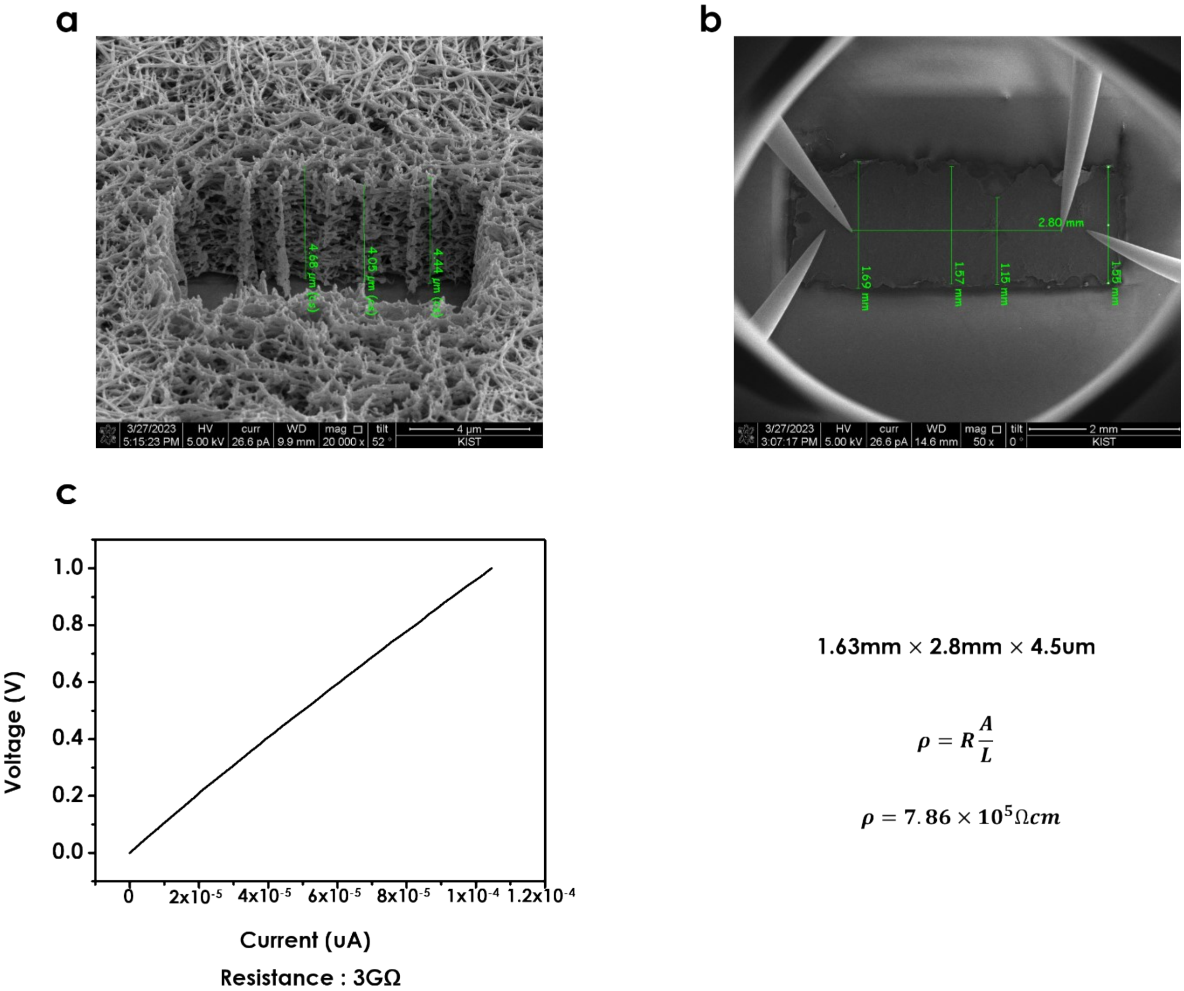

1.63mm × 2.8mm × 4.5um

$$\rho = R\frac{A}{L}$$

$$\rho = 7.86 \times 10^5 \Omega cm$$

Figure S17. a), b) SEM image of MTCP electrode cut by FIB in order to measure the electrical resistance. c) I-V curve of MTCP electrode prepared using FIB.

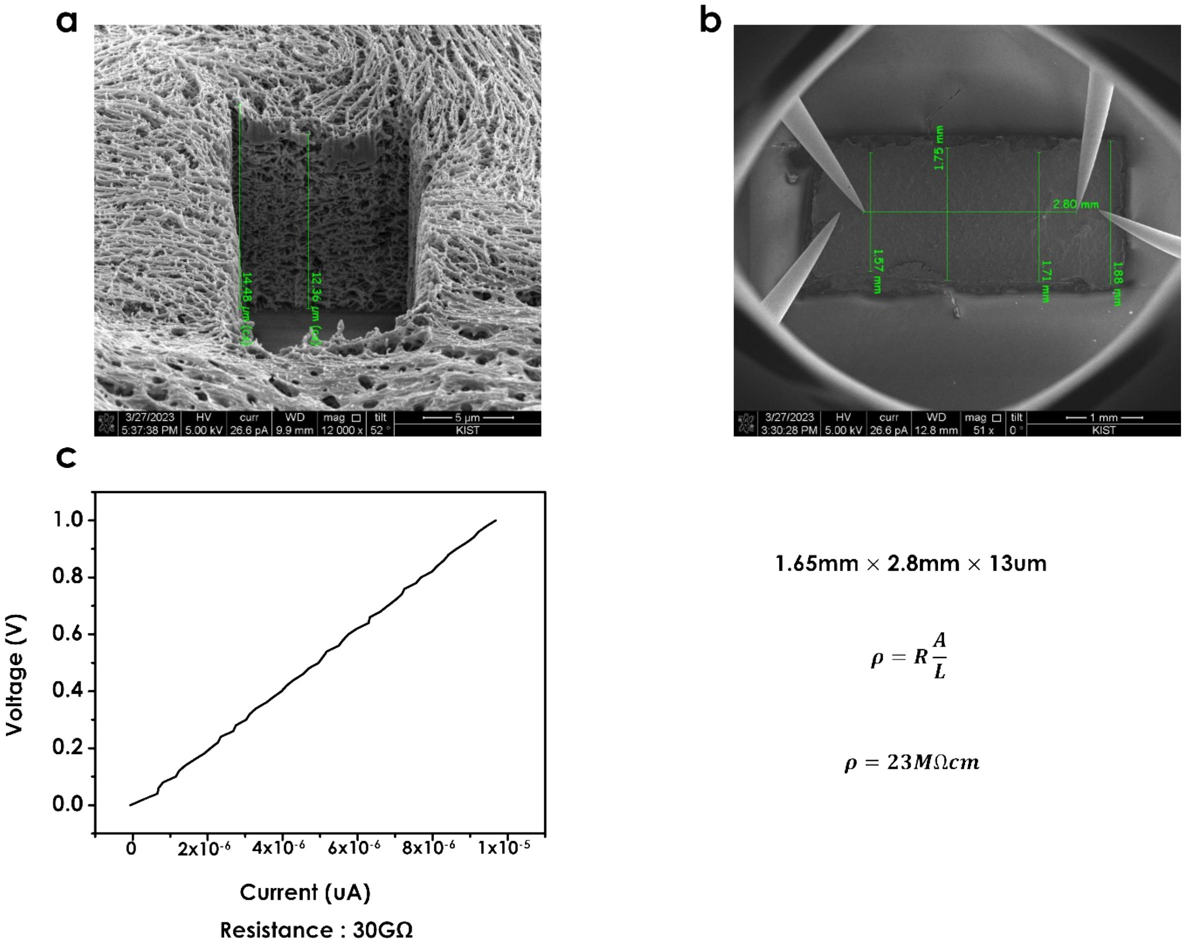

Resistance : 30GΩ

1.65mm × 2.8mm × 13um

$$\rho = R\frac{A}{L}$$

$$\rho = 23M\Omega cm$$

Figure S18. a), b) SEM image of Ag-MTCP electrode cut by FIB in order to measure the electrical resistance. c) I-V curve of Ag-MTCP electrode prepared using FIB.

Table S1. Atomic coordinates and equivalent isotropic displacement parameters for MTCP.

	X	***y***	***z***	B_{eq}
Cu1	0.7127	0.4712	0.4914	1
Cu2	0.2769	0.5008	0.4932	1
Cl1	0.9124	0.4124	0.4431	1
Cl2	0.9188	0.4228	0.9909	1
S1	0.6755	0.5876	0.7507	1
C1	0.7857	0.6930	0.7475	2.5
N1	0.9007	0.6626	0.7418	2.5
H1N	0.9191	0.5885	0.7281	2.5
H1M	0.9554	0.7136	0.7367	2.5
N2	0.7581	0.8081	0.7576	2.5
H2N	0.6855	0.8271	0.7626	2.5
C2	0.8451	0.9036	0.7627	2.5
H2A	0.8967	0.8937	0.8718	2.5
H2B	0.8936	0.9013	0.6492	2.5
H2C	0.8039	0.9804	0.7705	2.5
S2	0.3166	0.3849	0.7618	1
C3	0.1983	0.2888	0.7530	2.5
N3	0.0862	0.3282	0.7606	2.5
H3N	0.0735	0.4039	0.7578	2.5
H3M	0.0273	0.2821	0.7537	2.5
N4	0.2167	0.1716	0.7465	2.5
H4N	0.2876	0.1469	0.7431	2.5
C4	0.1224	0.0833	0.7468	2.5
H4A	0.0750	0.0913	0.8608	2.5
H4B	0.0710	0.0955	0.6380	2.5
H4C	0.1573	0.0034	0.7415	2.5

Table S2. Sensing performance of various room temperature NH_3 sensors.

Material		**NH_3 concentration (ppm)**	**Gas response (%)**	**Response time (s)**	**Recovery time (s)**	**ref**
MTCP		100	915	403	711	This work
Ag-MTCP		100	1925	378	215	This work
Metal oxide based	CuO	200	14.17	250	90	3
	ZnO-MWCNT	10	1.022	13.7	107.1	4
	$Ti_3C_2T_x$ /GO/CuO/ZnO	100	59.9	26	25	5
	Nd-doped SnO_2 film	25	68.2	27	6	6
Polymer based	PPy/f-MWCNT	100	26.5	16	110	7
	PPy nanostructures	100	34.25	23	57	8
	PPy-MXene	100	31.9	38	383	9
2D material based	CuO decorated WS_2	10	76.1	x	805	10
	Black phosphorus	100	121	22	220	11
	S defects WS_2	100	4.61	x	435.6	12
Si based	self-aligned SiNWs	100	75.8	360	1440	13
PANI based	PANI/MoS_2/SnO_2	100	990	21	130	14
	PANI/$SrGe_4O_9$	10	208	108	320	15
	$CoFe_2O_4$/PANI	100	1200	18	31	16
	PANI@Ag	100	77	18	15	17
	WS_2@PANI	100	216.3	25	39	18
	PANI/$Ti_3C_2T_X$/TiO_2	10	2.3	266	342	19

References

1. G. M. Sheldrick, *Acta Crystallogr., Sect. C: Struct. Chem.*, 2015, **71**, 3-8.
2. G. M. Sheldrick, *Acta Crystallogr., Sect. A: Found. Adv.*, 2015, **71**, 3-8.
3. G. Chaloeipote, R. Prathumwan, K. Subannajui, A. Wisitsoraat and C. Wongchoosuk, *Mater. Sci. Semicond. Process.*, 2021, **123**, 105546.
4. L. Vatandoust, A. Habibi, H. Naghshara and S. M. Aref, *Synth. Met.*, 2021, **273**, 116710.
5. Y. Seekaew, S. Kamlue and C. Wongchoosuk, *ACS Appl. Nano Mater.*, 2023, **6**, 9008-9020.
6. S. Maheswari, M. Karunakaran, L. B. Chandrasekar, K. Kasirajan and N. Rajkumar, *J. Mater. Sci.: Mater. Electron.*, 2020, **31**, 12586-12594.
7. S. D. Lawaniya, S. Kumar, Y. Yu and K. Awasthi, *ACS Appl. Polym. Mater.*, 2023, **5**, 1945-1954.
8. S. D. Lawaniya, S. Kumar, Y. Yu and K. Awasthi, *Sens. Actuators, B*, 2023, **382**, 133566.
9. P. Chen, Z. Zhao, Z. Shao, Y. Tian, B. Li, B. Huang, S. Zhang, C. Liu and X. Shen, *J. Mater. Sci.: Mater. Electron.*, 2022, **33**, 6168-6177.
10. H. Luo, J. Shi, C. Liu, X. Chen, W. Lv, Y. Zhou, M. Zeng, J. Yang, H. Wei, Z. Zhou, Y. Su, N. Hu and Z. Yang, *Nanotechnology*, 2021, **32**, 445502.
11. D. Han, X. Han, X. Zhang, W. Wang, D. Li, H. Li and S. Sang, *Sens. Actuators, B*, 2022, **367**, 132038.
12. Z. Qin, X. Song, J. Wang, X. Li, C. Wu, X. Wang, X. Yin and D. Zeng, *Appl. Surf. Sci.*, 2022, **573**, 151535.
13. X. Song, R. Hu, S. Xu, Z. Liu, J. Wang, Y. Shi, J. Xu, K. Chen and L. Yu, *ACS Appl. Mater. Interfaces*, 2021, **13**, 14377-14384.
14. A. Liu, S. Lv, L. Jiang, F. Liu, L. Zhao, J. Wang, X. Hu, Z. Yang, J. He, C. Wang, X. Yan, P. Sun, K. Shimanoe and G. Lu, *Sens. Actuators, B*, 2021, **332**, 129444.
15. Y. Zhang, J. Zhang, Y. Jiang, Z. Duan, B. Liu, Q. Zhao, S. Wang, Z. Yuan and H. Tai, *Sens. Actuators, B*, 2020, **319**, 128293.
16. Z. Wang, X. Chang, J. Li, X. Zhu, Y. Zhang, D. Wang, Y. Jiang and S. Sun, *Mater. Res. Bull.*, 2024, **175**, 112774.
17. A. Verma and T. Kumar, *Polyhedron*, 2024, **255**, 116982.
18. P. Wang, C. Tang, H. Song, L. Zhang, Y. Lu and F. Huang, *ACS Appl. Mater. Interfaces*, 2024, **16**, 14082-14092.
19. J. Xiong, Y. Cai, X. Nie, Y. Wang, H. Song, H. M. A. Sharif, Z. Li and C. Li, *Sens. Actuators, B*, 2023, **390**, 133987.